Geophysical Research Letters

RESEARCH LETTER
10.1029/2022GL100924

Key Points:

- Previously neglected drought feedbacks initiated by water deficits in the subsurface are prolonging water deficits
- The shortfall of subsurface water leads to higher clouds via changes in the sensible heat flux
- Higher clouds let more solar radiation reach the ground contributing to drought persistence

Supporting Information:

Supporting Information may be found in the online version of this article.

Correspondence to:

C. Hartick,
c.hartick@fz-juelich.de

Citation:

Hartick, C., Furusho-Percot, C., Clark, M. P., & Kollet, S. (2022). An interannual drought feedback loop affects the surface energy balance and cloud properties. *Geophysical Research Letters*, *49*, e2022GL100924. https://doi.org/10.1029/2022GL100924

Received 19 AUG 2022
Accepted 28 OCT 2022

An Interannual Drought Feedback Loop Affects the Surface Energy Balance and Cloud Properties

Carl Hartick[1,2], Carina Furusho-Percot[1,2,3], Martyn P. Clark[4], and Stefan Kollet[1,2]

[1]Agrosphere (IBG-3), Research Centre Jülich, Jülich, Germany, [2]Centre for High-Performance Scientific Computing in Terrestrial Systems, Geoverbund ABC/J, Jülich, Germany, [3]Now at INRAe, Avignon, France, [4]University of Saskatchewan Coldwater Laboratory, Canmore, AB, Canada

Abstract Long-term groundwater droughts are known to persist over timescales from multiple years up to decades. The mechanisms leading to drought persistence are, however, only partly understood. Applying a unique terrestrial system modeling platform in a probabilistic simulation framework over Europe, we discovered an important positive feedback mechanism from groundwater into the atmosphere that may increase drought persistence at interannual time scales over large continental regions. In the feedback loop, groundwater drought systematically increases net solar radiation via a cloud feedback, which, in turn, increases the drying of the land. In commonly applied climate and Earth system models, this feedback cannot be simulated due to a lack of groundwater memory effects in the representation of terrestrial hydrology. Thus, drought persistence and compound events may be underestimated in current climate projections.

Plain Language Summary Depending on the climate zone, droughts can persist for a very long time. In generally dry regions, interactions between the drought and the atmosphere become quickly apparent with a missing moisture supply from the surface. In more humid areas like the mid-latitudes, the effects are more hidden because there is more guarantee for moisture supply from the ocean. Still, some feedbacks prolong droughts that are often overlooked in climate modeling. We show with a model that includes the whole water cycle from the groundwater to the cloud top that drought conditions can change the properties of the clouds with changes in the energy cycle. The clouds become higher and transmit more solar energy to the surface. The surplus of energy at the surface leads to more evaporation and prolonged droughts.

1. Introduction

Droughts are part of the observed natural variability of the water cycle acting over large spatial scales and on time scales from weeks to decades (Peterson et al., 2021). Factors that influence hydrologic drought are precipitation deficits, hydrologic memory effects, land use modifications (Staal et al., 2020), human water use (Wada et al., 2013), and climate change (Samaniego et al., 2018). In addition, non-linear feedback loops, for example, the triggering of mesoscale circulations or changed advection patterns may be critical in connecting hydrologic drought with atmospheric processes in the terrestrial system (Seneviratne et al., 2010).

The feedback of soil moisture with land surface temperature and precipitation via evapotranspiration has been studied previously (Humphrey et al., 2018; Miralles et al., 2019; Zhou et al., 2021), showing connections at the weather and climatological time scales (Guo et al., 2006; Koster et al., 2006). Simulating relevant feedbacks can both rely on complex groundwater formulations (Keune et al., 2016) or high-resolution atmospheric models that enable explicit convective processes (Hohenegger et al., 2009). Both come with additional computational costs.

Central Europe is usually not water-limited (Stegehuis et al., 2013) and local feedback processes are superposed by large-scale atmospheric processes. However, during summer and under drought conditions, the influence of local feedbacks may increase (Phillips & Klein, 2014), because the whole energy balance at the surface is shifted toward dominance of the sensible over the latent heat flux (LH) (Rajan et al., 2015). Possible consequences are changes in surface albedo with changed soil color due to decreasing soil moisture and vegetation (Meng et al., 2014). Shifts in the energy balance also increase the sensible heat flux (SH), which can influence the cloud base and cover via interactions with the boundary layer (Ardilouze et al., 2019; Betts, 2004). The upper part of the boundary layer is heated, leading to an extension, which moves the cloud base upwards. Dirmeyer et al. (2014) found a strengthened connection between sensible heat and the cloud base in climate projections of coupled models. Feedback processes like this might not only be critical in future climates but be relevant during current

droughts. In this study, with fully coupled groundwater-to-atmosphere simulations, positive feedback mechanisms between groundwater drought and atmospheric processes were discovered at the interannual time scale.

2. Data and Methods

2.1. Modeling System

The feedbacks between continental-scale groundwater and atmospheric processes are examined using coupled land-atmosphere models (Barlage et al., 2015). In this study, we applied the Terrestrial Systems Modeling Platform (TSMP) consisting of coupled groundwater, land, and atmosphere models (Gasper et al., 2014; Shrestha et al., 2014).

The atmospheric part of TSMP is covered by the Consortium for Small-scale Modeling (COSMO) v5.01, a regional atmospheric model developed by multiple weather services under the leadership of the German Weather Service (Baldauf et al., 2011). In TSMP, COSMO provides precipitation, temperature, humidity, horizontal winds, air pressure, shortwave energy and longwave energy fluxes to the land scheme based on the Community Land Model (CLM) version 3.5.

In return, in the coupled framework, CLM (Oleson et al., 2004, 2008) provides COSMO with upwelling longwave and reflected shortwave energy, turbulent momentum, moisture and energy fluxes, which are calculated for individual grid cells. Relevant processes in CLM are evaporation, root water uptake and transpiration, and sensible heat, which are parameterized based on thermodynamic, plant physiologic and similarity theory. In this study, the connection of these processes to shallow soil moisture and groundwater redistribution, which is calculated by the variably saturated groundwater and surface water flow model ParFlow, is key in explaining the feedback.

ParFlow (Ashby & Falgout, 1996; Jones & Woodward, 2001; Kollet & Maxwell, 2006; Maxwell, 2013) solves the 3D Richards-equation for a physical representation of variably saturated groundwater flow, which enables the calculation of for example, total water storage and groundwater table depth. Overland flow is represented with a kinematic wave equation in a free surface boundary condition. ParFlow covers the shallow soil layers in CLM and is extended with five additional soil layers to include deeper groundwater flow. At the upper boundary, ParFlow receives precipitation after interception and evapotranspiration from CLM. ParFlow provides subsurface water pressure potential and saturation values to CLM. The coupling of the different model components is implemented with OASIS3-MCT (Valcke, 2013). All models run independently managed by the coupler with variables exchanged in 2D and 3D arrays in memory (Gasper et al., 2014; Shrestha et al., 2014).

2.2. Model Setup and Reference Climatology

The global simulation domain encompasses the official EURO-CORDEX region (Giorgi et al., 2009; Gutowski et al., 2016), including large parts of continental Europe (Figure S1 in Supporting Information S1). The horizontal grid spacing is 0.11° on a rotated longitude-latitude grid, roughly equal to a distance of 12.5 km. The vertical grid spacing is variable, with the atmosphere reaching up to 22 km with 50 levels and the subsurface up to 57 m with 10 levels shared with CLM and ParFlow and five additional ParFlow layers. The subsurface grid is terrain following with increasing layer thickness with depth. Not resolving convection explicitly, we operate with the two-category ice scheme of COSMO that includes the categories of water vapor, cloud water (CLW), cloud ice, rain and snow. The convective parametrization from Tiedtke (1989) is utilized with the addition that mixed-phase clouds of ice and water are accounted for. Calculation of radiative fluxes is performed according to Ritter and Geleyn (1992), which enables the calculation of incoming solar radiation to the surface, taking into account partial cloudiness of individual layers and the water content in different forms through all layers. Generally, the timestep of COSMO is 60 s, while the CLM and ParFlow run with a timestep of 900 s, which is also the coupling frequency.

The lateral boundary information for the atmospheric model was obtained from the reanalysis data set ERA-Interim (Dee et al., 2011), updated every 3 hr at the domain's borders. Parameters for PFTs of CLM were obtained from the Moderate Resolution Imaging Spectroradiometer database (Friedl et al., 2002). The individual plant properties were calculated from the CLM surface data set. The topographic representation in ParFlow is represented by slopes in 2D derived from the United States Geological Survey GTOPO30 (DAAC, 2004), soil properties stem from the Food and Agriculture Organization of the United Nations database (Carballas et al., 1990) categorized

in 15 soil types with assumed vertical homogeneity. Due to the resolution of 12.5 km, there was the need to scale horizontal permeability by a factor of 1000 (Fang et al., 2016; Niedda, 2004). Along the coastlines, we apply a Dirichlet boundary condition for ParFlow with constant hydraulic pressure and a very shallow water table.

Applying ERA-Interim boundary forcing, a continuous climatologic time series was simulated from 1996 to 2019 with TSMP, which serves as the reference (REF) in this study. REF constitutes a consistent, transient climatology of all relevant states and fluxes of the terrestrial water and energy cycle from groundwater across the land surface into the atmosphere (Furusho-Percot et al., 2019). We focused on the region of Mid-Europe (ME) defined in Christensen and Christensen (2007) (Figure S1 in Supporting Information S1).

2.3. Ensemble Construction and Increment Analyses

In the ME focus region, there were three major groundwater drought events in the years 2011, 2018, and 2019 that were identified from anomalies of total subsurface water storage, S. These events were part of previous evaluation studies where water states and fluxes simulated with TSMP underwent a century-long spin up period and were shown to agree well with observations from remote sensing (Furusho-Percot et al., 2019; Hartick et al., 2021).

We applied an established probabilistic ensemble prediction approach (Day, 1985; Wood & Lettenmaier, 2008), which can be summarized as follows: To assess the impact of drought conditions at the end of a given water year (1 September–31 August) on the hydrologic and atmospheric system in the ensuing water year, the atmospheric uncertainty must be taken into account at the interannual time scale. Since there is arguably no predictive skill in for example, precipitation at the interannual time scale, an ensemble of atmospheric conditions must be constructed that covers the full range of atmospheric uncertainty, which encompasses, in the best case, realizations of all possible atmospheres for the ensuing water year. In this study, an estimate of atmospheric uncertainty was obtained by forcing the ensuing water year with atmospheric ERA-Interim boundary conditions of the 22 water years, $y \in Y = \{1996, 1997, ..., 2018\}$ covering the simulated time series of the reference simulation, REF. Thus, a single initial drought condition at the end of a water year resulted in an ensemble of 22 realizations of the hydrologic and atmospheric system in the ensuing water year over the simulation domain. With three drought years considered the total ensemble size was 66. Note, the initial disequilibrium between the atmospheric and hydrologic system right at the beginning of each simulation after initialization can be neglected, because of the strong dynamics and short memory of the atmosphere on the order of hours to days. For more details on the experimental design, the reader is referred to Hartick et al. (2021)

The ensemble results were analyzed based on increments $\Delta_{Y,V}$, where the subscript V is a set of subsurface, land surface, and atmospheric variables $v \in V = \{\text{RNET, LH, SH, GH, SSR, LF, CEILING, CLT, LCL, CLW}\}$ defined in Section 2.4; and Y is the set of REF forcing years defined above. Individual increments were calculated as the differences between the ensemble members initialized with the drought conditions of the years $i \in I = \{2011, 2018, 2019\}$ and REF simulation results for the years Y (Figure S2 in Supporting Information S1)

$$\Delta_{y,v} = v_{y,i} - v_{y,REF} \quad (1)$$

In the analyses, all $\Delta_{Y,V}$ were seasonally and spatially averaged over the focus region and normalized with the seasonal standard deviation (background atmospheric variability) of REF over the focus region resulting in the averaged increment Δv for a given variable $v \in V$. Thus, Δv reflect the impact of initial drought conditions on land surface and atmospheric variables at the interannual time scale. If the increments, Δv, follow a normal distribution with a mean of zero (essentially white noise), this would suggest that the drought initial conditions do not have a systematic impact on V. Thus, essentially the null hypothesis is tested, which, in case of rejection, suggests that indeed a systematic influence of drought initial conditions on V may exist. In the testing, we used the standard t-test, Bayesian networks (Salvatier et al., 2016), and bootstrapping (Figure S3 in Supporting Information S1).

2.4. Key Climate Variables

In the analyses, we inspected increments, Δv, defined in Section 2.3 of the land surface energy budget including net radiation at the surface (RNET), SH, LH, and ground heat flux (GH). Further, we inspected the net values of incoming shortwave (SSR) and longwave radiation (LF) at the surface. SSR is determined by the solar radiation coming from COSMO and the ground albedo calculated in CLM. LF is estimated from ground

temperature and cloud cover. Overall, SSR simulated by TSMP agreed well with the independent reanalysis product ERA5-Land (Muñoz-Sabater et al., 2021) (Figure S4 in Supporting Information S1). To calculate the water deficit in the subsurface, all soil layers are added to the total subsurface water storage, S. For cloud-related variables, we analyzed the cloud ceiling height (CEILING), total cloud cover (CLT), lifting condensation level (LCL) and CLW content. CEILING is the height at which most of the sky is covered with clouds, which can also be observed by ceilometers. COSMO has been evaluated against such observations reaching high values of reproducibility (Bucchignani & Mercogliano, 2021). CEILING is a measure for cloud height both in convective and high-pressure synoptic situations, where cirrus clouds are formed. Under clear-sky conditions, CEILING reaches an arbitrary maximum value which we removed from the analyses. LCL is a useful variable in convective situations describing the level to which an air parcel near the surface needs to be lifted to reach supersaturation and start forming a cloud. LCL does not exist as a direct model output, but Romps (2017) derived exact solutions for LCL from pressure, humidity and temperature at the surface (TAS), which we use to calculate it. CLW is the amount of water stored in clouds with a negligible fall velocity serving as a reservoir for precipitable water. Comparisons to observations are difficult because the amount of CLW is small and difficult to separate from the total amount of water in the atmosphere. The variable is more useful in the modeling realm, especially in parameterizations of subgrid-scale cloudiness. CLW is also part of widely applied reanalysis products like ERA5 (Hersbach et al., 2020), with which TSMP agrees well (Figure S5 in Supporting Information S1).

3. Results

Figure 1 shows the essential result of the probabilistic numerical experiment. In Figures 1a–1c, all energy increments normalized by their background atmospheric variability of one standard deviation are positive or close to zero. The full energy balance including fluxes with non-significant increments is found in the Supporting Information (Figure S6 in Supporting Information S1). For example, the mean ΔRNET in summer is about 25% of the natural variability with the range reaching 100%. Thus, in the simulations with dry initial conditions, more energy is absorbed by the land surface than in REF. This energy is mainly partitioned into SH with the mean ΔSH being close to 50% of the natural variability with an even larger range. Analyses of in situ energy flux observations during the extreme European summer of 2018 also identified sensible heat as the most affected flux of the energy cycle (Graf et al., 2020). Decomposing the net energy balance at the surface into its components ΔSSR (Figure 1c) and ΔLF (Figure S6F in Supporting Information S1), the results show an increase in incoming shortwave radiation in the mean sense and a decrease in LF in case of drought initial conditions. There is a mean increase of around 2.5 W m^{-2} for ΔSSR in absolute numbers. Compared to the natural variance, this is of considerable magnitude, especially considering the impact can be much higher in individual years. Overall the probability of a positive increment in ΔSSR increases to about 70% (Figure S8 in Supporting Information S1). Principal component analysis (Geladi & Kowalski, 1986), which has been used to study coupling strengths (Zhou et al., 2021), shows that a more negative ΔS leads to a stronger increment in net solar radiation in most regions of Europe (Table S1 in Supporting Information S1). The darker shaded boxplots in Figure 1 denote in which seasons the results significantly differ statistically according to a single mean two-sided *t*-test. The results support the finding that significant, systematic changes are detectable only for SH, RNET and SSR in summer; other energy balance components, ΔGH and ΔLH (Figures S6D and S6F in Supporting Information S1), did not show a systematic change for the different drought initial conditions.

The positive ΔRNET and ΔSSR increments suggest that changes in the energy fluxes have to be connected to not only differences in surface albedo but altered cloud properties. This modification is interrogated with cloud-related variables in Figures 1d–1f. Most notably, the cloud height is consistently higher with an average absolute CEILING increment of some 110 m, which is on the order of the natural variability (Figure 1d). To a lesser degree, CLT is also consistently reduced by about 25% of the natural variability (Figure S9B in Supporting Information S1). These two variables include all types of clouds, such as high cirrus clouds, low stratocumulus and convective clouds. The changes in cloud height seem to be the most consistent change in the ensembles with all assembled increments being significant, thus, supporting the suggested feedback loop. Inspection of convective processes (Figure 1e) shows the increments in the LCL, ΔLCL. Absolute LCL values were calculated for every grid cell individually from relative humidity (RELHUM), pressure and temperature and then spatially aggregated and seasonally averaged. The values of ΔLCL indicate that changes in convective cloud generation appear to be especially important in summer with the mean close to 50% natural variability and passing the p-value threshold. While near-surface temperatures are mainly unchanged (Figure S7B in Supporting Information S1), the changes

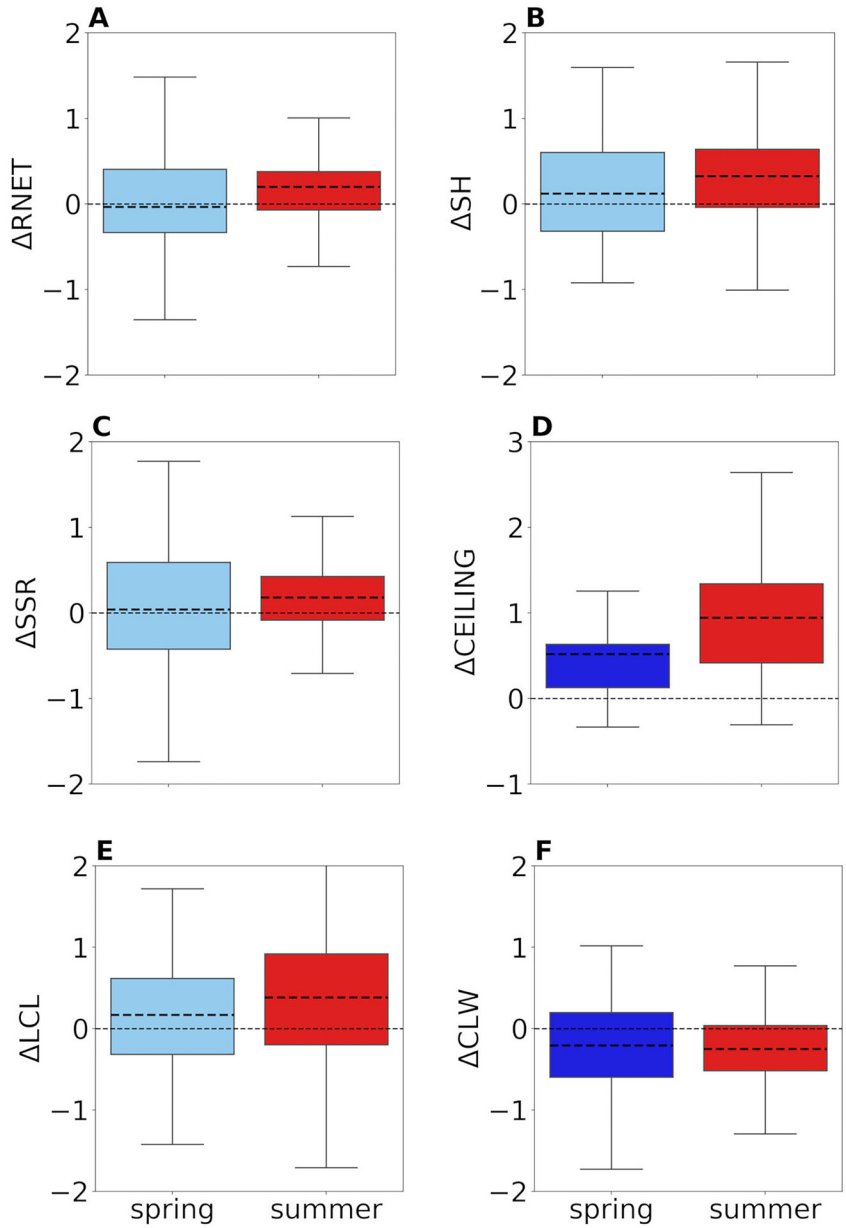

Figure 1. Boxplots of the normalized increments of the energy and cloud variables in spring and summer of the drought experiments. The net surface energy flux RNET (a) is shown with its component the sensible heat flux (b). (c) Shows the net energy fluxes of shortwave radiation SSR. (d–f) depict cloud-related variables, including cloud ceiling height CEILING (d), the lifting condensation level (e) and total cloud water content (f). Light blue and red denote ensembles that did not pass a single mean two-sided *t*-test (p-value > 0.05). Negative values indicate a deficit in the experiments, positive values a surplus. The dotted line inside the boxes shows the average of the increments.

in RELHUM (Figure S7C in Supporting Information S1) induce changes in LCL. We also identified a systematic reduction in total CLW CLW (Figure 1f) while precipitation (PR) remains unchanged (Figure S7D in Supporting Information S1) due to the strong chaotic nature of precipitation-generating processes.

These results lead us to formulate a positive feedback loop induced by significant groundwater storage deficits at the interannual time scale (Figure 2). Strong memory effects of groundwater storage deficits increase the probability of drought persistence in the ensuing year. Drought conditions change the land surface energy balance, increasing the sensible heat due to an initially reduced LH because of lower water availability. A large-scale increase in sensible heat increases the energy input of the atmosphere, shifting the boundary layer and cloud

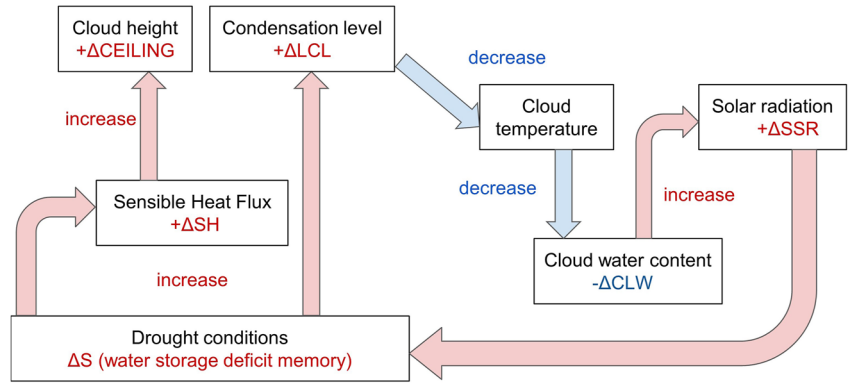

Figure 2. Schematic of feedback mechanism. ΔSH, ΔCEILING, ΔCLW, ΔSSR, and ΔLCL indicate the significant increments of sensible heat flux, cloud height and cloud water content, identified as the long-term effects of drought initial conditions ΔS.

height upwards to lower temperatures, where clouds have reduced water content. The drought conditions also increase the LCL through lower humidity near the surface. Higher thin clouds with reduced cloud cover transmit more solar radiation to the surface, increasing net solar radiation and lowering downward LF. Thus, in the positive feedback loop, modification of cloud cover characteristics is key in increasing incoming radiation at the land surface.

The temporal onset of the feedback loop in the water year via an initial change in energy partitioning is not easily detectable at the seasonal timescale. However, there is an indication for the onset of the feedback loop at the daily timescale with opposite development of ΔLH and ΔSH at the beginning of the summer season in June (Figure S10 in Supporting Information S1). ΔSH shows a persistent surplus, while ΔLH increments are mainly negative. Following this opposite development, CLW was consistently reduced and SSR increased. Later in summer, the regime changed, both energy fluxes increase on average, reflecting the increase in solar radiation and available energy at the land surface. We also identified the onset and feedback in other mid-latitude regions over Europe, which likely interact at the continental scale (Figures S11 and S12 in Supporting Information S1).

Table 1
p-Value, Summer Mean, and Std of Reference and Mean Increments of Discussed Variables

Variable	p-value	REF mean	REF std	Mean Δ
CEILING	6.94E−13	8488.25 m	119.97 m	112.95 m
S	7.57E−09	23,687 mm	20.13 mm	−12.54 mm
SH	2.29E−05	29.82 W m^{-2}	3.19 W m^{-2}	1.03 W m^{-2}
CLW	4.43E−05	0.07 mm	0.02 mm	−0.004 mm
LCL	1.30E−03	352.08 m	10.43 m	3.99 m
CLT	1.56E−03	77.00%	4.00%	−0.01%
RNET	2.09E−03	97.67 W m^{-2}	6.74 W m^{-2}	1.35 W m^{-2}
SSR	4.00E−03	146.19 W m^{-2}	14.0 W m^{-2}	2.51 W m^{-2}
RELHUM	2.31E−02	76.93%	1.57%	−0.33%
LF	1.45E−01	50.02 W m^{-2}	5.34 W m^{-2}	−0.99 W m^{-2}
PR	2.00E−01	77.8 mm	12.23 mm	−1.48 mm
LH	3.55E−01	62.97 W m^{-2}	3.29 W m^{-2}	0.22 W m^{-2}
GH	7.36E−01	4.86 W m^{-2}	1.57 W m^{-2}	0.03 W m^{-2}
TAS	9.92E−01	288.11 K	0.97 K	−0.01 K

Note. p-values are obtained by sampling all summer increments with a single mean two-sided *t*-test. The null hypothesis is a mean of 0.

To provide context for the increments of all variables, Table 1 shows the p-value, the summer mean and standard deviation in REF and the mean increment of all discussed variables. Inspecting the order of magnitude, CEILING and S have the lowest p-value. The low value for S is intuitive, because it is a direct consequence of the applied drought initial conditions. The other variables in the feedback process (SH, CLW, LCL, CLT, RNET, SSR, and RELHUM) are roughly in the same order of magnitude. The low p-value of CEILING could be connected to other unknown atmospheric processes. The p-value of the remaining variables (LF, PR, LH, GH, and TAS) are not significant, thus not directly influenced by the drought initial condition at the interannual time scale.

In Figure 3a, the exemplary spatial inspection of the increments for the drought conditions of 2018 shows that the impact and memory effect of the applied initial drought conditions on ΔS in the following summer are widespread but spatially heterogeneous. Mean ΔSSR (Figure 3b) in summer is spatially more homogeneous suggesting modifications of characteristics in atmospheric conditions that cannot be attributed to spatially continuous changes of land surface albedo. The grid cell-wise correlation between ΔS and ΔSSR is negative for most of the domain (Figure 3c), corroborating previous conclusions that more negative deficits lead to higher surpluses in net shortwave radiation. Exceptions are positive values near northern coastal

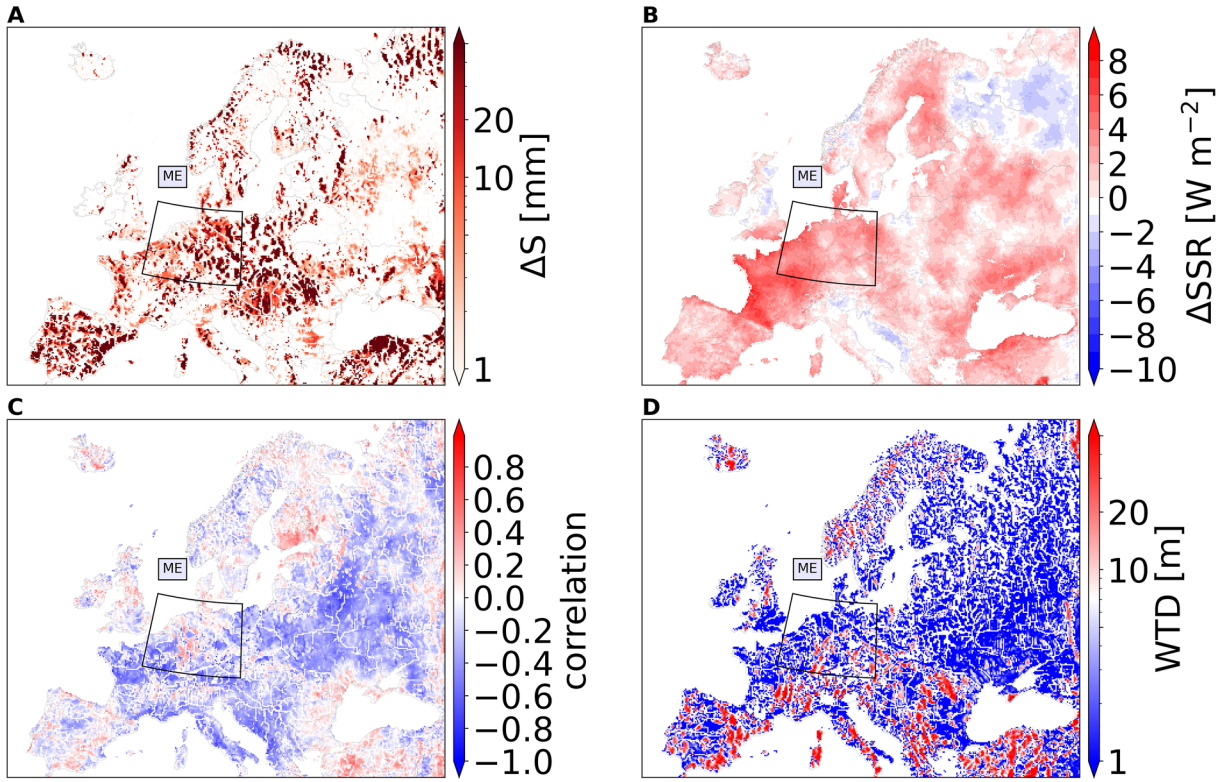

Figure 3. Spatial pattern of the mean increment of the 2018 experiment for the subsurface water storage deficits in summer in logarithmic scale (a), incoming solar radiation increment in the summer (b), and Pearson Correlation between the increments (c) and the average water table depth in the domain from the year 1996 to 2018 illustrated on logarithmic scale (d). Mid-Europe indicates the focus region of the study.

regions, which can be explained by shallow groundwater (Figure 3d) along the modeled coastlines, which are more likely to experience less deficits and recover faster due to groundwater convergence.

4. Conclusions

For the first time, the presented ensemble simulations demonstrate positive hydrologic drought feedback of groundwater storage deficits on atmospheric processes related to cloud processes and radiation at the interannual timescale in the mid-latitudes. The net solar radiation is systematically larger in the summer months following groundwater drought conditions in the previous fall. Thus, groundwater drought potentially enters a positive feedback loop with cloud-forming processes and incoming solar radiation in successive years, increasing the probability of drought persistence. Evidence exists for the proposed feedback loop in observational and reanalysis data for the Canadian great plains (Greene et al., 2011) and China (Zeng et al., 2019), emphasizing the global relevance. Over Europe, similar feedbacks involving reduced soil moisture have been identified in climate projections, however primarily attributed to changes in the LH (Vogel et al., 2018). In this study, the identified feedback loop is based on simulation results and, thus, impacted by uncertainties related to input parameters, and simplifying model assumptions and parametrizations at the respective spatial resolution on the order of 10 km. While TSMP has been evaluated in previous studies with observations showing good agreement and a high degree of physical realism (Furusho-Percot et al., 2019; Hartick et al., 2021) the proposed feedback loop has not been evaluated directly. Corroboration of the identified feedback loop under widespread drought conditions with observations would require future studies to connect field measurements with remote sensing data. In Earth system modeling, global and most regional climate models do not capture groundwater memory effects. Thus, current climate modeling studies might underestimate the temporal persistence of droughts and compound events.

Data Availability Statement

The data used in the study are available at https://datapub.fz-juelich.de/slts/prob_cordex/data/.

Acknowledgments
The study received funding from the Helmholtz RSF Joint Research Group and the Initiative and Networking Fund of the Helmholtz Association (HGF) through the project "Advanced Earth System Modeling Capacity (ESM)". The content of the paper is the sole responsibility of the author(s) and does not represent the opinion of the Helmholtz Assosication, and the Helmholtz is not responsible for any use that might be made of the infromation contained. The authors gratefully acknowledge the ESM project for funding this work by providing computing time on the ESM partition of the supercomputer JUWELS at the Jülich Supercomputing Center (JSC). Open Access funding enabled and organized by Projekt DEAL.

References

Ardilouze, C., Batté, L., Déqué, M., van Meijgaard, E., & van den Hurk, B. (2019). Investigating the impact of soil moisture on European summer climate in ensemble numerical experiments. *Climate Dynamics*, *52*(7–8), 4011–4026. https://doi.org/10.1007/s00382-018-4358-1

Ashby, S. F., & Falgout, R. D. (1996). A parallel multigrid preconditioned conjugate gradient algorithm for groundwater flow simulations. *Nuclear Science and Engineering*, *124*(1), 145–159. https://doi.org/10.13182/NSE96-A24230

Baldauf, M., Seifert, A., Foerstner, J., Majewski, D., Raschendorfer, M., & Reinhardt, T. (2011). Operational convective-scale numerical weather prediction with the COSMO model: Description and sensitivities. *Monthly Weather Review*, *139*(12), 3887–3905. https://doi.org/10.1175/MWR-D-10-05013.1

Barlage, M., Tewari, M., Chen, F., Miguez-Macho, G., Yang, Z. L., & Niu, G. Y. (2015). The effect of groundwater interaction in North American regional climate simulations with WRF/Noah-MP. *Climatic Change*, *129*(3–4), 485–498. https://doi.org/10.1007/s10584-014-1308-8

Betts, A. K. (2004). Understanding hydrometeorology using global models. *Bulletin of the American Meteorological Society*, *85*(11), 1673–1688. https://doi.org/10.1175/BAMS-85-11-1673

Bucchignani, E., & Mercogliano, P. (2021). Performance evaluation of high-resolution simulations with COSMO over south Italy. *Atmosphere*, *12*(1), 45. https://doi.org/10.3390/atmos12010045

Carballas, T., Macias, F., Diaz-Fierros, F., Carballas, M., & Fernandez-Urrutia, J. A. (1990). FAO-UNESCO soil map of the world. Revised legend. *Informes Sobre Recursos Mundiales de Suelos (FAO)*.

Christensen, J. H., & Christensen, O. B. (2007). A summary of the PRUDENCE model projections of changes in European climate by the end of this century. *Climatic Change*, *81*(1), 7–30. https://doi.org/10.1007/s10584-006-9210-7

Daac, L. P. (2004). *Global 30 arc-second elevation data set GTOPO30*. Land Process Distributed Active Archive Center.

Day, G. N. (1985). Extended streamflow forecasting using NWSRFS. *Journal of Water Resources Planning and Management*, *111*(2), 157–170. https://doi.org/10.1061/(asce)0733-9496(1985)111:2(157)

Dee, D. P., Uppala, S. M., Simmons, A. J., Berrisford, P., Poli, P., Kobayashi, S., et al. (2011). The ERA-Interim reanalysis: Configuration and performance of the data assimilation system. *Quarterly Journal of the Royal Meteorological Society*, *137*(656), 553–597. https://doi.org/10.1002/qj.828

Dirmeyer, P. A., Wang, Z., Mbuh, M. J., & Norton, H. E. (2014). Intensified land surface control on boundary layer growth in a changing climate. *Geophysical Research Letters*, *41*(4), 1290–1294. https://doi.org/10.1002/2013GL058826

Fang, Z., Bogena, H., Kollet, S., & Vereecken, H. (2016). Scale dependent parameterization of soil hydraulic conductivity in 3D simulation of hydrological processes in a forested headwater catchment. *Journal of Hydrology*, *536*, 365–375. https://doi.org/10.1016/J.JHYDROL.2016.03.020

Friedl, M. A., McIver, D. K., Hodges, J. C. F., Zhang, X. Y., Muchoney, D., Strahler, A. H., et al. (2002). Global land cover mapping from MODIS: Algorithms and early results. *Remote Sensing of Environment*, *83*(1–2), 287–302. https://doi.org/10.1016/S0034-4257(02)00078-0

Furusho-Percot, C., Goergen, K., Hartick, C., Kulkarni, K., Keune, J., & Kollet, S. (2019). Pan-European groundwater to atmosphere terrestrial systems climatology from a physically consistent simulation. *Scientific Data*, *6*(1), 320. https://doi.org/10.1038/s41597-019-0328-7

Gasper, F., Goergen, K., Shrestha, P., Sulis, M., Rihani, J., Geimer, M., & Kollet, S. (2014). Implementation and scaling of the fully coupled Terrestrial Systems Modeling Platform (TerrSysMP v1.0) in a massively parallel supercomputing environment—A case study on JUQUEEN (IBM Blue Gene/Q). *Geoscientific Model Development*, *7*(5), 2531–2543. https://doi.org/10.5194/gmd-7-2531-2014

Geladi, P., & Kowalski, B. R. (1986). Partial least-squares regression: A tutorial. *Analytica Chimica Acta*, *185*, 1–17. https://doi.org/10.1016/0003-2670(86)80028-9

Giorgi, F., Jones, C., Asrar, G. R., & others (2009). Addressing climate information needs at the regional level: The CORDEX framework. *World Meteorological Organization Bulletin*, *58*(3), 175.

Graf, A., Klosterhalfen, A., Arriga, N., Bernhofer, C., Bogena, H., Bornet, F., et al. (2020). Altered energy partitioning across terrestrial ecosystems in the European drought year 2018: Energy partitioning in the drought 2018. *Philosophical Transactions of the Royal Society B: Biological Sciences*, *375*(1810), 20190524. https://doi.org/10.1098/rstb.2019.0524

Greene, H., Leighton, H. G., & Stewart, R. E. (2011). Drought and associated cloud fields over the Canadian Prairie provinces. *Atmosphere-Ocean*, *49*(4), 356–365. https://doi.org/10.1080/07055900.2011.559771

Guo, Z., Dirmeyer, P. A., Koster, R. D., Sud, Y. C., Bonan, G., Oleson, K. W., et al. (2006). GLACE: The global land--atmosphere coupling experiment. Part II: Analysis. *Journal of Hydrometeorology*, *7*(4), 611–625. https://doi.org/10.1175/jhm511.1

Gutowski, J. W., Giorgi, F., Timbal, B., Frigon, A., Jacob, D., Kang, H. S., et al. (2016). WCRP COordinated regional downscaling EXperiment (CORDEX): A diagnostic MIP for CMIP6. *Geoscientific Model Development*, *9*(11), 4087–4095. https://doi.org/10.5194/gmd-9-4087-2016

Hartick, C., Furusho-Percot, C., Goergen, K., & Kollet, S. (2021). An interannual probabilistic assessment of subsurface water storage over Europe using a fully coupled terrestrial model. *Water Resources Research*, *57*(1). https://doi.org/10.1029/2020WR027828

Hersbach, H., Bell, B., Berrisford, P., Hirahara, S., Horányi, A., Muñoz-Sabater, J., et al. (2020). The ERA5 global reanalysis. *Quarterly Journal of the Royal Meteorological Society*, *146*(730), 1999–2049. https://doi.org/10.1002/qj.3803

Hohenegger, C., Brockhaus, P., Bretherton, C. S., & Schär, C. (2009). The soil moisture-precipitation feedback in simulations with explicit and parameterized convection. *Journal of Climate*, *22*(19), 5003–5020. https://doi.org/10.1175/2009JCLI2604.1

Humphrey, V., Zscheischler, J., Ciais, P., Gudmundsson, L., Sitch, S., & Seneviratne, S. I. (2018). Sensitivity of atmospheric CO_2 growth rate to observed changes in terrestrial water storage. *Nature*, *560*(7720), 628–631. https://doi.org/10.1038/s41586-018-0424-4

Jones, J. E., & Woodward, C. S. (2001). Newton-Krylov-multigrid solvers for large-scale, highly heterogeneous, variably saturated flow problems. *Advances in Water Resources*, *24*(7), 763–774. https://doi.org/10.1016/S0309-1708(00)00075-0

Keune, J., Gasper, F., Goergen, K., Hense, A., Shrestha, P., Sulis, M., & Kollet, S. (2016). Studying the influence of groundwater representations on land surface-atmosphere feedbacks during the European heat wave in 2003. *Journal of Geophysical Research: Atmospheres*, *121*(22), 13301–13325. https://doi.org/10.1002/2016JD025426

Kollet, S. J., & Maxwell, R. M. (2006). Integrated surface-groundwater flow modeling: A free-surface overland flow boundary condition in a parallel groundwater flow model. *Advances in Water Resources*, *29*(7), 945–958. https://doi.org/10.1016/j.advwatres.2005.08.006

Koster, R. D., Guo, Z., Dirmeyer, P. A., Bonan, G., Chan, E., Cox, P., et al. (2006). GLACE: The global land-atmosphere coupling experiment. Part I: Overview. *Journal of Hydrometeorology*, *7*(4), 590–610. https://doi.org/10.1175/JHM510.1

Maxwell, R. M. (2013). A terrain-following grid transform and preconditioner for parallel, large-scale, integrated hydrologic modeling. *Advances in Water Resources*, *53*, 109–117. https://doi.org/10.1016/j.advwatres.2012.10.001

Meng, X. H., Evans, J. P., & McCabe, M. F. (2014). The influence of inter-annually varying albedo on regional climate and drought. *Climate Dynamics*, *42*(3–4), 787–803. https://doi.org/10.1007/s00382-013-1790-0

Miralles, D. G., Gentine, P., Seneviratne, S. I., & Teuling, A. J. (2019). Land–atmospheric feedbacks during droughts and heatwaves: State of the science and current challenges. *Annals of the New York Academy of Sciences*, *1436*(1), 19–35. https://doi.org/10.1111/nyas.13912

Muñoz-Sabater, J., Dutra, E., Agustí-Panareda, A., Albergel, C., Arduini, G., Balsamo, G., et al. (2021). ERA5-Land: A state-of-the-art global reanalysis dataset for land applications. *Earth System Science Data*, *13*(9), 4349–4383. https://doi.org/10.5194/essd-13-4349-2021

Niedda, M. (2004). Upscaling hydraulic conductivity by means of entropy of terrain curvature representation. *Water Resources Research*, *40*(4), 1–16. https://doi.org/10.1029/2003WR002721

Oleson, K. W., Dai, Y., Bonan, G. B., Bosilovich, M., Dickinson, R. E., Dirmeyer, P. A., et al. (2004). Technical description of the community land model (CLM) (Vol. *186*). NCAR Technical Note, *NCAR/TN*-46. https://doi.org/10.5065/D6N877R0

Oleson, K. W., Niu, G. Y., Yang, Z. L., Lawrence, D. M., Thornton, P. E., Lawrence, P. J., et al. (2008). Improvements to the community land model and their impact on the hydrological cycle. *Journal of Geophysical Research: Biogeosciences*, *113*(G1). https://doi.org/10.1029/2007JG000563

Peterson, T. J., Saft, M., Peel, M. C., & John, A. (2021). Watersheds may not recover from drought. *Science*, *372*(6543), 745–749. https://doi.org/10.1126/science.abd5085

Phillips, T. J., & Klein, S. A. (2014). Land-atmosphere coupling manifested in warm-season observations on the U.S. southern great plains. *Journal of Geophysical Research: Atmospheres*, *119*(2), 509–528. https://doi.org/10.1038/175238c0

Rajan, N., Maas, S. J., & Cui, S. (2015). Extreme drought effects on summer evapotranspiration and energy balance of a grassland in the Southern Great Plains. *Ecohydrology*, *8*(7), 1194–1204. https://doi.org/10.1002/eco.1574

Ritter, B., & Geleyn, J.-F. (1992). A comprehensive radiation scheme for numerical weather prediction models with potential applications in climate simulations. *Monthly Weather Review*, *120*(2), 303–325. https://doi.org/10.1175/1520-0493(1992)120<0303:acrsfn>2.0.co;2

Romps, D. M. (2017). Exact expression for the lifting condensation level. *Journal of the Atmospheric Sciences*, *74*(12), 3891–3900. https://doi.org/10.1175/JAS-D-17-0102.1

Salvatier, J., Wiecki, T. V., & Fonnesbeck, C. (2016). Probabilistic programming in Python using PyMC3. *PeerJ Computer Science*, *2*, e55. https://doi.org/10.7717/peerj-cs.55

Samaniego, L., Thober, S., Kumar, R., Wanders, N., Rakovec, O., Pan, M., et al. (2018). Anthropogenic warming exacerbates European soil moisture droughts. *Nature Climate Change*, *8*(5), 421–426. https://doi.org/10.1038/s41558-018-0138-5

Seneviratne, S. I., Corti, T., Davin, E. L., Hirschi, M., Jaeger, E. B., Lehner, I., et al. (2010). Investigating soil moisture-climate interactions in a changing climate: A review. *Earth-Science Reviews*, *99*(3–4), 125–161. https://doi.org/10.1016/j.earscirev.2010.02.004

Shrestha, P., Sulis, M., Masbou, M., Kollet, S., & Simmer, C. (2014). A scale-consistent terrestrial systems modeling platform based on COSMO, CLM, and ParFlow. *Monthly Weather Review*, *142*(9), 3466–3483. https://doi.org/10.1175/MWR-D-14-00029.1

Staal, A., Flores, B. M., Aguiar, A. P. D., Bosmans, J. H. C., Fetzer, I., & Tuinenburg, O. A. (2020). Feedback between drought and deforestation in the Amazon. *Environmental Research Letters*, *15*(4), 44024. https://doi.org/10.1088/1748-9326/ab738e

Stegehuis, A. I., Vautard, R., Ciais, P., Teuling, A. J., Jung, M., & Yiou, P. (2013). Summer temperatures in Europe and land heat fluxes in observation-based data and regional climate model simulations. *Climate Dynamics*, *41*(2), 455–477. https://doi.org/10.1007/s00382-012-1559-x

Tiedtke, M. (1989). A comprehensive mass flux scheme for cumulus parameterization in large-scale models. *Monthly Weather Review*, *117*(8), 1779–1800. https://doi.org/10.1175/1520-0493(1989)117<1779:ACMFSF>2.0.CO;2

Valcke, S. (2013). The OASIS3 coupler: A European climate modelling community software. *Geoscientific Model Development*, *6*(2), 373–388. https://doi.org/10.5194/gmd-6-373-2013

Vogel, M. M., Zscheischler, J., & Seneviratne, S. I. (2018). Varying soil moisture-atmosphere feedbacks explain divergent temperature extremes and precipitation projections in central Europe. *Earth System Dynamics*, *9*(3), 1107–1125. https://doi.org/10.5194/esd-9-1107-2018

Wada, Y., Van Beek, L. P. H., Wanders, N., & Bierkens, M. F. P. (2013). Human water consumption intensifies hydrological drought worldwide. *Environmental Research Letters*, *8*(3), 034036. https://doi.org/10.1088/1748-9326/8/3/034036

Wood, A. W., & Lettenmaier, D. P. (2008). An ensemble approach for attribution of hydrologic prediction uncertainty. *Geophysical Research Letters*, *35*(14), 1–5. https://doi.org/10.1029/2008GL034648

Zeng, D., Yuan, X., & Roundy, J. K. (2019). Effect of teleconnected land-atmosphere coupling on northeast China persistent drought in spring-summer of 2017. *Journal of Climate*, *32*(21), 7403–7420. https://doi.org/10.1175/JCLI-D-19-0175.1

Zhou, S., Williams, A. P., Lintner, B. R., Berg, A. M., Zhang, Y., Keenan, T. F., et al. (2021). Soil moisture–atmosphere feedbacks mitigate declining water availability in drylands. *Nature Climate Change*, *11*(1), 38–44. https://doi.org/10.1038/s41558-020-00945-z